Supporting Information for

Nanostructured High-Performance Dielectric Block Copolymer

Wenmei Liu,[a] Xiaojuan Liao,[a] Yawei Li,[b] Qiuhua Zhao,[a] Meiran Xie*[a] and Ruyi Sun*[a]

Materials

Tricyclohexylphosphine[1,3-bis(2,4,6-trimethylphenyl)-4,5-dihydroimidazol-2-ylidene] benzylidene ruthenium dichloride (**Ru-II**), norbornene-5,6-*endo*-dicarboxylic anhydride (NDA), lithium aluminum hydride ($LiAlH_4$), 3,5-difluoroaniline, pentafluorophenol 4-dimethylaminopyridine (DMAP), and 1-(3-dimethylaminopropyl)-3-ethylcarbodiimide hydrochloride (EDCI·HCl) were purchased from Sigma-Aldrich or Energy Chemical Co. and used as received without purification. $CHCl_3$, Ethyl acetate (EtOAc), hexane, ethanol, methanol, and magnesium sulfate ($MgSO_4$) were purchased from Shanghai Chemical Reagents Co., and used as received without purification. [1,3-Bis(2,4,6-trimethylphenyl)-4,5-dihydroimidazol-2-ylidene][3-bromo-pyridine]$_2$ benzylidene ruthenium dichloride (**Ru-III**)[1] and 4-carboxyl-1,6-heptadiyne[2] were prepared according to the known synthetic procedures in the related literatures. Solvents were distilled over drying agents under nitrogen prior to use: Chloroform ($CHCl_3$), dichloromethane (CH_2Cl_2) and dichloroethene (DCE) from calcium hydride; THF from sodium/benzophenone. All reactions were carried out under dry nitrogen atmospheres using standard Schlenk-line techniques.

Characterization

^{1}H NMR (500 MHz), ^{13}C NMR (125 MHz), and ^{19}F NMR (500 MHz) spectra were recorded on a Bruker DPX spectrometer using tetramethylsilane as an internal standard in $CDCl_3$. UV-vis absorption spectra were measured on a UV-1800 spectrometer with the concentration of 1.0×10^{-3} mg mL^{-1}. IR spectra were recorded on a Perkin Elmer Spectrum using KBr pellets. The HRMS was measured by a Bruker QTOF micromass spectrometer. Differential scanning calorimeter (DSC) was performed on a Netzsch 204F1 in nitrogen atmosphere. An indium standard was used for temperature and enthalpy calibrations. All the samples were first heated from 30 to 200 ^{o}C and held at this temperature for 3 min to eliminate the thermal history, and then, they were cooled to room temperature and heated again from 30 to 200 ^{o}C at a heating or cooling rate of 10 ^{o}C min^{-1}. Gel permeation chromatography (GPC) was used to calculate relative molecular weight and molecular weight distribution equipped with a Waters 1515 Isocratic HPLC pump, a Waters 2414 refractive index detector, and a set of Waters Styragel columns (7.8 × 300 mm, 5 mm bead size; 10^3, 10^4, and 10^5 Å pore size). GPC measurements were carried out at 35 ^{o}C using THF as the eluent with a flow rate of 1.0 mL/min. The system was calibrated with monodispersed polystyrene standards. X-ray diffraction (XRD) analysis was performed on a Rigaku D/MAX2400 diffractometer. Elemental analysis was conducted with an Elementar vario EL. Transmission electron microscopy (TEM) images were recorded on the JEOL2100F microscopes operating at 120 kV. Samples for TEM measurement were prepared by depositing a drop of $CHCl_3$ or THF solution with different concentration on the copper grids coated with carbon, followed by air-drying. Additionally, the samples were not stained before measurement because the electron density difference between the two blocks provided sufficient contrast for TEM imaging. The hydrodynamic diameter was determined by means of dynamic light scattering (DLS) analysis using a Malvern Zetasizer Nano-ZS light scattering apparatus (Malvern Instruments, U.K.) with a He-Ne laser (633 nm, 4 mW). The Nano ZS instrument incorporates noninvasive backscattering (NIBS) optics with a detection angle of 173^o. The z-average diameter of the sample was automatically provided by the instrument using cumulate analysis. Film qualities of copolymers were observed by a field emission scanning electron microscopy (FESEM) (HITACHI S4800). Dielectric analysis was conducted on a Novo control BDS40 dielectric spectrum analyzer at room temperature, and a contacting electrode method was used. Measurements were carried out at low applied voltage (typically 10 mV) and varying frequency (typically 100 Hz to 1 MHz) for 3−5 specimens of each sample to ensure reproducibility. The edge side (d) of the guarded electrode is 0.3 mm. The capacitance (C_p) and the dissipation factor (dielectric loss, loss tangent) of the tested films were recorded and the data were interpreted using a parallel RC circuit model expected to describe a “leaky” capacitor. Polarization measurements at higher applied voltages employed a polarization tester (Precision Multiferroic, Radiant, Inc.). The electric displacement (D)–electric field (E) hysteresis loops were recorded for applied voltages up to 100 V with a cycle frequency of 100 Hz.

Sample preparation for dielectric measurements

Polymer was dissolved in $CHCl_3$ to a solution of 10 wt% for dielectric impendence measurements and 1 wt% for polarization measurements, and then, the solution was stirred for 12 h at room temperature, followed by the sonication for 10 min. After that, the solution was spin-coated on ITO substrate at spinning speed of 1000-1500 rpm for 60 s, and dried in air overnight, followed by continuous heat treatment (40 ^oC) in vacuum for another 12 h to evaporate all the solvents. The thickness of film was controlled by using different solution concentration and spinning speed, and tested by the Elcometer

(Veeco Dektak 6M). The typical thicknesses of the polymer films were about 1.2 μm and about 100 nm for dielectric impendence measurements and polarization measurements, respectively. And then, a thin layer (500 Å) of Pt particle was sputtered on the exposure sides of the sample. The dielectric constant ε can be calculated by equation: $\varepsilon = C_pt/\varepsilon_0A$; where t is the thickness of the film and ε_0, the permittivity of the free space, is 8.85×10^{-12} F/m, A is the guarded electrode area, $A = d^2$. The electric field can be calculated by equation: $E = U/t$, where U is the voltage, t is the thickness of the film.

Synthesis of N-3,5-difluorophenyl-norbornene-dicarboximide ***(FNDI)****:* 3,5-difluoroaniline (6.45 g, 50 mmol) and norbornene-5,6-*endo*-dicarboxylic anhydride (NDA) (3.15 g, 19.2 mmol) were dissolved in 80 mL of DCE. DMAP (1.83 g, 15 mmol) was then added to the stirred solution at room temperature and the mixture was further refluxed at 90 °C for 36 h. After that, the solution was washed by dilute hydrochloric acid (3 × 30 mL), followed by water (3 × 30 mL), and dried with anhydrous $MgSO_4$. After filtration and removing the solvent, a white needle crystal was obtained by recrystallization twice from ethanol (11.2 g, 81.5% yield). M.p. 147-148 °C; ^{1}H NMR (500 MHz, $CDCl_3$, 25°C, TMS): δ = 6.83-6.78 (m, 3H, o-ArH, p-ArH), 6.25 (s, 2H, C*H*=C*H*CH), 3.52 (s, 2H, CHC*H*C=O), 3.43 (s, 2H, CHC*H*CH_2), 1.81-1.77 and 1.65-1.60 ppm (dd, J = 9.0 and 10.5 Hz, 2H, CHCH_2CH); ^{13}C NMR (125 MHz, $CDCl_3$, 25°C, TMS): δ = 175.93 (CH*C*=O), 163.66 (CH*C*F), 161.79 (N*C*CH), 134.66 (*C*H=CHCH), 110.04 (NC*C*H), 104.1 (FC*C*HCF), 52.29 (CH*C*H_2CH), 45.75, 45.61 ppm (CH*C*HC=O + CH*C*HCH_2); ^{19}F NMR (500 MHz, $CDCl_3$, 25°C, TMS): δ = -111.05 ppm.

Synthesis of N-3,5-difluorophenyl-norbornene-pyrrolidine ***(FNP)***: to a suspension of $LiAlH_4$ (4.56 g, 120 mmol) in Et_2O (100 mL), **FNDI** (6.7 g, 24 mmol) in anhydrous CH_2Cl_2 (80 mL) was added dropwise under nitrogen atmosphere at 0 °C, and the mixture was stirred at room temperature for 24 h. EtOAc (10 mL) and then water (5 mL) was carefully introduced to quench excess $LiAlH_4$. The resulting suspension was filtered, and the residue was washed with CH_2Cl_2 repeatedly. The organic phase was dried with $MgSO_4$ and the solvent was removed in vacuo to give the crude product as a gray solid. After recrystallization from a mixture of hexane and EtOAc (3:1) for three times, the product was obtained in a white crystal (4.3 g, 72% yield). M.p. 67-69 °C; ^{1}H NMR (500 MHz, $CDCl_3$, 25°C, TMS): δ = 6.18-6.05 (m, 3H, o-ArH, p-ArH), 5.94-5.91 (m, 2H, C*H*=C*H*CH), 3.22-3.06 (m, 4H, CHCH_2N), 2.98 (s, 2H, CHC*H*CH_2), 2.86-2.82 (C*H*CHCH_2N), 1.63-1.60 and 1.53-1.51 ppm (dd, J = 8.5 and 10.0 Hz, 2H, CHCH_2CH);

^{13}C NMR (125 MHz, $CDCl_3$, 25°C, TMS): δ = 163.17, 164.81 (CH*C*F), 149.13 (N*C*CH), 135.76 (*C*H=CHCH), 94.59 (NC*C*H), 90.26 (FC*C*HCF), 52.09 (CH*C*H_2N), 50.71 (CH*C*H_2CH), 46.56 (CH*C*HCH_2), 45.40 ppm (CH*C*HCH_2N); ^{19}F NMR (125 MHz, $CDCl_3$, 25°C, TMS): δ = -111.05 ppm; HRMS (ESI): calcd for $C_{15}H_{16}F_2N$: 248.1292; found, 248.1245; elemental analysis calcd (%) for $C_{15}H_{16}F_2N$: C 72.86, H 6.11, N 5.66; found: C 72.40, H 6.10, N 5.90.

Synthesis of pentafluorophenyl-functionalized 1,6-heptadiyne ***(FHD)***: 4-carboxyl-1,6-heptadiyne (3.2 g, 20 mmol) was firstly dissolved in 60 mL of anhydrous CH_2Cl_2. To this solution, pentafluorophenol (2.2 g, 24 mmol), DMAP (0.5 g, 4 mmol), and EDCI·HCl (4.6 g, 24 mmol) were sequentially added under a nitrogen atmosphere in ice-water bath, then the reaction proceeded at room temperature and was monitored by TLC. After 3 days, the mixture was washed with deionized water (3 × 30 mL) and saturated NaCl solution (3 × 30 mL). The organic layer was dried over anhydrous $MgSO_4$. Solvent was then evaporated to give the crude product as a yellowish solid. After recrystalization from a mixture of hexane and ethyl acetate twice, the product was obtained in a white crystal (4.30 g, 64% yield). M.p. 48.5-49.4 °C. ^1H NMR (500 MHz, $CDCl_3$, 25°C, TMS): δ = 3.18 (m, 1H, OCOCH), 2.83-2.81 (m, 4H, CHCC*H_2*), 2.14 ppm (t, 2H, C*H*CCH_2); ^{13}C NMR (125 MHz, $CDCl_3$, 25°C, TMS): δ = 168.51 (CH*C*OO), 142.04-136.89 (*C*F=*C*F*C*F), 79.06 (CH*C*CH_2), 71.43 (*C*HCCH_2), 43.11 (CH_2*C*HCO), 19.99 ppm (CHC*C*H_2); ^{19}F NMR (500 MHz, $CDCl_3$, 25°C, TMS): δ = -152.4, -157.6, -162.1 ppm.

General procedure for polymerizations

Syntheses of homopolymers via ROMP

Homopolymers were prepared by ROMP using **Ru-III** as the catalyst and a typical procedure was as follows. In a dry nitrogen-filled Schlenk tube, a solution of **Ru-III** (8.8 mg, 0.01 mmol) in 1 mL of CH_2Cl_2, which was degassed in three freeze-vacuum-thaw cycles, was added to a degassed solution of monomer **FNDI** (185.3 mg, 0.75 mmol) in 2.7 mL of CH_2Cl_2 to give a monomer concentration of 0.2 mol/L. After 10 min, the polymerization was quenched by adding a drop of ethyl vinyl ether with stirring for 30 min, and then precipitated into an excess of methanol. Polymer was dissolved in $CHCl_3$, and precipitated once again from methanol. The obtained polymer poly(N-3,5-difluorophenyl-norbornene-dicarboximide) (**PFNDI**) was dried in a vacuum oven at 40 °C to a constant weight. ^1H NMR (500 MHz, $CDCl_3$, 25°C, TMS) for **PFNDI**: δ = 7.01-6.74 (m, p-ArH and o-ArH), 5.85-5.63 (m, 5.85-5.72 for *trans*-C*H*=C*H* and 5.72-

5.63 for *cis*-C*H*=C*H* on polymer chain), 3.50-3.16 (m, CHC=O), 3.15-2.95 (m, CH=CHC*H*), 2.03-1.91 and 1.51-1.33 ppm (m, CHCH_2CH); GPC data for **PFNDI**: M_n = 7.8 kDa, M_w/M_n = 1. 13.

^{1}H NMR (500 MHz, $CDCl_3$, 25°C, TMS) for **PFNP**: δ = 6.23-5.98 (m, p-ArH and o-ArH), 5.44-5.32 (m, *trans*-C*H*=C*H* on polymer chain), 3.31-3.00 (m, CHCH_2N), 2.99-2.84 (m, CH=CHC*H*), 2.85-2.71 (m, CHC*H*CH_2), 1.91-1.75 and 1.51-1.33 ppm (m, CHCH_2CH); GPC data for **PFNP**: M_n = 20.6 kDa, M_w/M_n = 1. 12.

Syntheses of block copolymers via tandem ROMP and MCP

The block copolymers were prepared by ROMP followed by MCP with the sequential addition of monomers, and a typical procedure was as follows. In a nitrogen-filled Schlenk tube, a solution of **Ru-III** (8.8 mg, 0.01 mmol) in 1 mL of THF, which was degassed in three freeze-vacuum-thaw cycles, was added to a degassed solution of the first monomer **FNP** (185.2 mg, 0.75 mmol) in 2.7 mL of THF to give a monomer concentration of 0.2 mol/L. After stirring for 10 min at 30 °C, a degassed solution of the second monomer **FHD** (45.2 mg, 0.15 mmol) in 0.2 mL of CH_2Cl_2 was then added under nitrogen. After stirring for 1 h, the polymerization was quenched by adding a drop of ethyl vinyl ether with stirring for further 30 min, and the solution was then poured into an excess of methanol. The polymer was redissolved in CH_2Cl_2, and precipitated once again from methanol. The precipitate was dried under vacuum for 24 h at 40 °C to a constant weight. (500 MHz, $CDCl_3$, 25°C, TMS): δ = 6.19-5.98 (m, p-ArH and o-ArH), 5.49-5.32 (m, *trans*-C*H*=C*H* on polymer chain), 3.33-2.67 (m, CHCH_2N + CH=CHC*H* + CHC*H*CH_2), 1.99-1.75 and 1.53-1.33 ppm (m, CHCH_2CH); GPC data for **PFNP**$_{75}$-*b*-**PFHD**$_{25}$: M_n = 24.8 kDa, M_w/M_n = 1. 11.

Syntheses and characterization of monomers

The functional monomers **FNDI** and **FNP** were synthesized starting from the reaction of NDA with 3,5-difluoroaniline in the presence of catalyst DMAP in DCE at refluxed temperature, firstly achieved **FNDI**, which was then easily transformed into **FNP** by reduction reaction with $LiAlH_4$. Two crude products were purified by recrystallization from ethanol to give a white crystal, and then characterized by ^{1}H, ^{13}C, and ^{19}F NMR spectroscopy, HR-ESIMS, and element analysis. The ^{1}H NMR spectra of **FNDI** and **FNP** (Figures S1a and S1c) indicated the presence of characteristic double band (proton b) at 6.24 ppm on the norbornene ring and the phenyl group (protons e and f) at 6.84-6.74 ppm, and the integration ratio for these two types of protons was 2:2.98, which was agreed well with the theoretical value of 2:3. Also, ^{19}F NMR spectra (Figures S2a and S2b) showed the single resonance signal at -111.05 ppm. These are indicative of 3,5-difluoroaniline group being connected to the norbornene ring. Moreover, ^{1}H NMR spectrum of **FNP** (Figure S1c) showed new resonance signals appeared at 3.23-3.06 ppm from two groups of methylene (proton g) adjacent to the norbornene ring in contrast to the ^{1}H NMR spectrum of **FNDI**, meant carbonyl group was completely reduced to methylene. In ^{13}C NMR spectrum of **FNDI** (Figure S1b), the resonance of carbonyl carbons appeared at 176.30 ppm, and the signals at 163.67, 167.41, and 104.07 ppm were contributed to the carbons of C_i, C_h, and C_f on phenyl groups, respectively. In ^{13}C NMR spectrum of **FNP** (Figure S1d), the signals of carbonyl carbons disappeared and new resonance of methylene carbons (C_g) observed at 51.92 ppm, which also evidenced the complete reduction of **FNDI** to **FNP**.

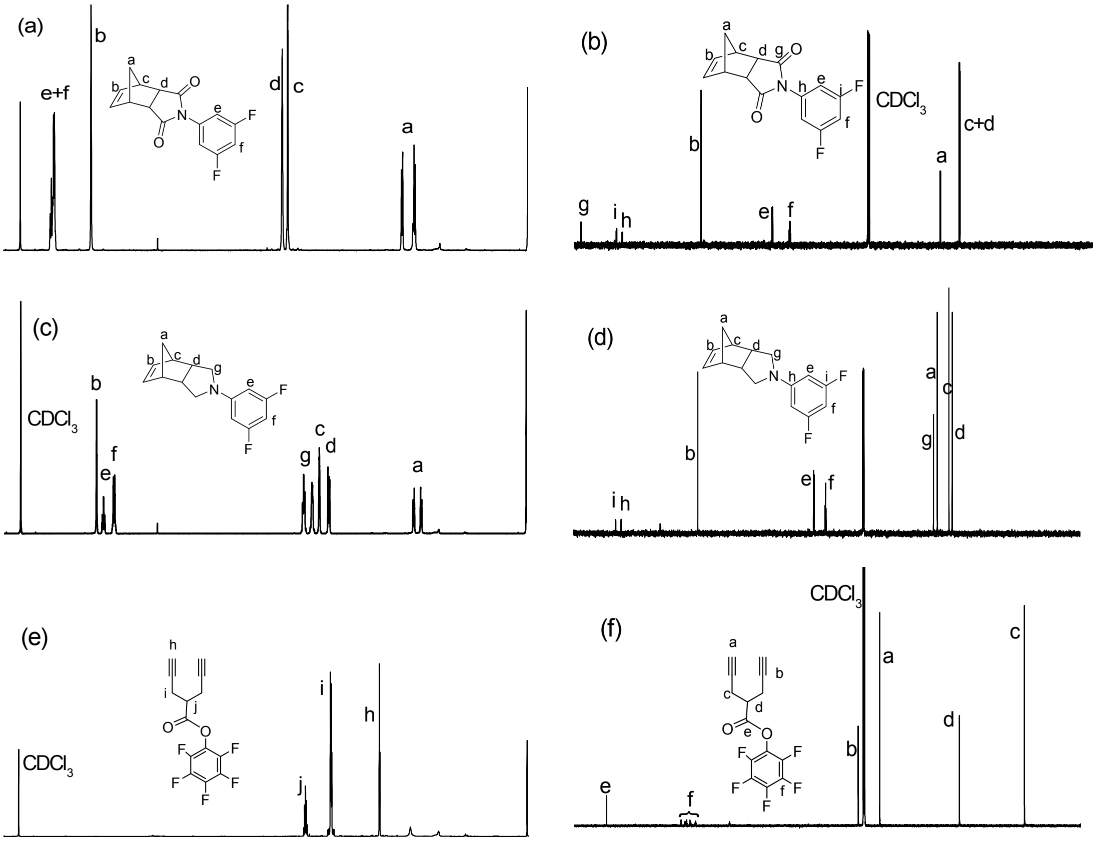

Figure S1. ^{1}H NMR spectra of (a) **FNDI**, (c) **FNP**, and (e) **FHD**; ^{13}C NMR spectra of (b) **FNDI**, (d) **FNP,** and (f) **FHD**.

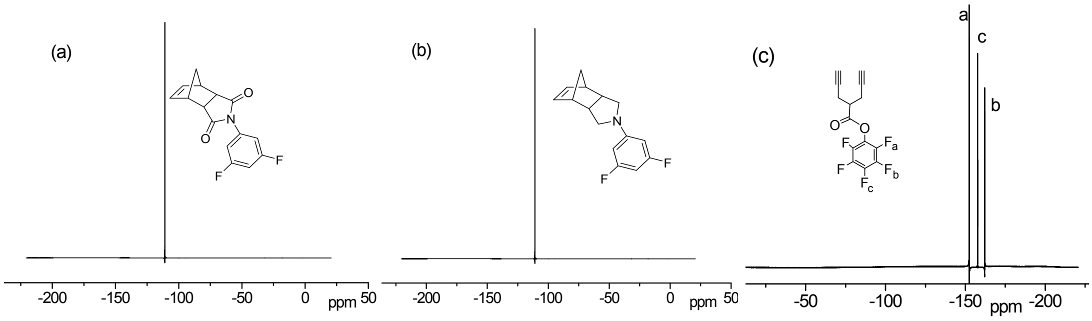

Figure S2. ^{19}F NMR spectra of (a) **FNDI**, (b) **FNP**, and (c) **FHD**.

Additionally, IR spectrum of **FNDI** showed the typical, characteristic C=O stretch band at 1779 and 1719 cm^{-1} (Figure S3a), while disappearance in the IR spectrum of **FNP** (Figure S3c), confirming the transformation of carbonyl into methylene successfully. Element analysis and HR-MS also indicated that both of the products have the right element content and molecular weight. Apparently, these points assured the successful preparation of **FNDI** and **FNP** with the expected structure.

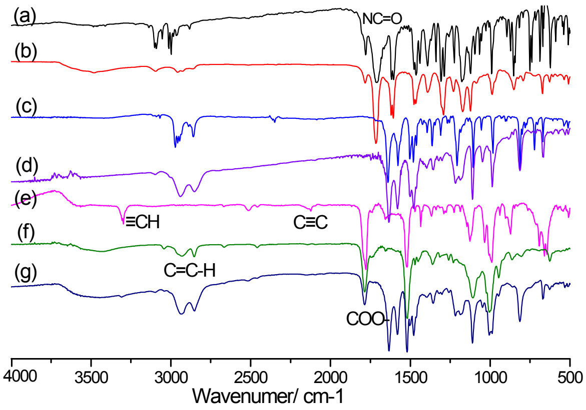

Figure S3. Infrared spectra of (a) **FNDI**, (b) **PFNDI**, (c) **FNP**, (d) **PFNP,** (e) **FHD**, (f) **PFHD**, and (g) **PFNP**$_{75}$-*b*-**PFHD**$_{25}$.

The monomer **FHD** was readily prepared by the conventional esterification reaction of pentafluorophenol and 4-carboxyl-1,6-heptadiyne using EDCI·HCl and DMAP as the catalyst system in CH_2Cl_2 at room temperature. The structure was tested by ^{1}H and ^{13}C NMR spectroscopy, IR, HRMS, and element analysis. In the ^{1}H NMR spectrum (Figure S1e), the resonance signals at 3.19 and 2.82 ppm can be assigned to methylene (protons i and j) of 4-carboxyl-1,6-heptadiyne, and 2.14 ppm is the characteristic peak of the terminal acetylenic proton. ^{13}C NMR spectrum of **FHD** was shown in Figure S1f, the peak at 71.1 ppm is attributed to acetylenic carbon, 168.7 ppm is assigned to the carbonyl carbon, and the carbons on phenyl group appeared at a range of 136.2-142.4 ppm because of C-F coupling. ^{19}F NMR spectrum (Figure S2c) showed the resonance signals at -152.4, -157.6, and -162.1 ppm. Additionally, IR spectrum (Figure S3e) showed both the acetylenic hydrogen stretching (3301 cm^{-1}) and the carbon-carbon triple-bond stretching (2122 cm^{-1}). HRMS and element analysis also indicated the product have the right element content and molecular weight. All of these points confirmed that **FHD** has been successfully synthesized with the expected chemical structure.

ROMP and MCP behaviors of monomers

Homopolymers **PFNDI** and **PFNP** were first synthesized by ROMP, **PFHD** was then generated via MCP, and block copolymer **PFNP**$_n$-*b*-**PFHD**$_m$ was finally obtained by means of the combination of ROMP and MCP using **Ru-III** as catalyst. The synthetic routes are shown in Figure 1a.

Initially, ROMP of **FNP** with molar feed ratio of **FNP** to **Ru-III** ([M]/[I]) of 75 (Table S1) was conducted in THF. When **Ru-III** was added to the solution of **FNP**, the colorless solution gradually changed to dark-yellow. After 10 min, the resultant polymer was obtained by precipitating the mixture from excess methanol with the molecule weight (M_n) of 20.6 kDa and narrow polydispersity index (PDI = 1.12) in 89% yield, indicating that **FNP** is of high activity for ROMP. For comparison, ROMP of monormer **FNDI** was conducted in CH_2Cl_2, while the isolated yield was only 65% and M_n was 7.8 kDa within 10 min. The less activity of dicarboximide **FNDI** than pyrrolidine **FNP** for ROMP probably caused by the steric interaction between the propagating ruthenium-center and the *endo*-ring of an incoming monomer.[3] As depicted above, **PFNP** can be served as an ideal candidate as the first block in preparation of block copolymer.

Table S1. Characteristics for polymerizations and the resultant polymers[a]

Run	[**FNP**]:[**FHD**]:[I][b]	Yield (%)	M_n[c] (kDa)	PDI[c]	M_n[d] (kDa)	PDI[d]
1	75:0:1	89	20.6	1.12	/	/
2	75:0:1[e]	65	7.8	1.13	/	/
3	0:25:1	87	/	/	/	/
4	100:50:1	81	/	/	/	/
5	75:50:1	88	31.9	1.19	318	1.38
6	75:25:1	86	24.8	1.11	272	1.40
7	75:15:1	89	24.4	1.19	219	1.27
8	50:25:1	83	23.6	1.18	244	1.28

[a] Polymerization conditions: T = 30 °C, Cat = **Ru-III**, solvent = THF, the initial concentration of **FNP** or **FNDI** = 0.2 mol/L, t = 10 min + 1 h. [b] The feed ratios of monomer **FNP** to monomer **FHD** and catalyst. [c] Molecular weight (M_n) and polydispersity index (PDI) of the single polymer chain determined by GPC using THF as eluent. [d] Molecular weight and polydispersity index corresponding to the aggregates of polymer chains determined by GPC using THF as eluent. [e] ROMP of **FNDI** instead of **FNP** was performed in CH_2Cl_2.

According the previous study, MCP of **FHD** was carried out with a molar feed ratio of **FHD** to **Ru-III** ([M]/[I]) of 25:1 in a weakly coordinating solvent of THF. At first trial, a violent reaction with a great deal of heat-releasing was observed when the concentration of **FHD** was at 0.2 mmol/mL at 30 ^{o}C and the reaction system immediately transformed from colorless solution to dark red solid, which was nearly insoluble in common organic solvents such as CH_2Cl_2, $CHCl_3$, and THF. Because of the poor solubility of homopolymer **PFHD**, no further characterization of NMR spectroscopy or size exclusion chromatography (GPC) was performed. However, the stretching vibration of unsaturated C≡C–H and C≡C was disappeared in IR spectrum of **PFHD** (Figure S3f). Additionally, the absorbance of homopolymer **PFNP** in $CHCl_3$ was observed at 240-300 nm in the UV-vis spectrum (Figure S4), corresponding to the phenyl pendant and the backbone of **PFNP**, which is different from that of monomer **FNP**. The appearance of weak characteristic absorption of PA backbone at 480 nm for the supernatant of **PFHD** solution is in contrast to that of monomer **FHD** without the UV-vis absorption, which further convinced that ROMP of **FNP** and MCP of **FHD** are succeeded.

It should be noted that solubility plays an important role in solution characterization of polymer and solution-processed organic electronic devices. As the poor solubility of **PFHD** was concerned, the diblock copolymer consisting of more soluble **PFNP** and less insoluble **PFHD** segments with the high feed ratio of 100:50 was synthesized by tandem ROMP and MCP to ensure the solubility and optimize the dielectric property of copolymers (Table S1, ESI†) and expected to improve the solubility and promote the dielectric property of copolymer. **FNP** was firstly polymerized in THF to yield living macro-initiators with 100 repeat units. After fully consumption of monomer monitored by TLC (within 10 min), **FHD** was added to this living macrospecies, and the solution color immediately changed from dark yellow to red when **FHD** was added, suggesting MCP of **FHD** happened. After another 60 min, the reaction was quenched by addition of ethyl vinyl ether and the polymer was purified by simple precipitation into methanol. The diblock copolymer was obtained in high isolated yield, and they possess a relatively good solubility in various organic solvents such as THF and CH_2Cl_2. Unluckily, GPC curve of the block copolymer showed a same trace as that of homopolymer **PFNP**, suggesting an incomplete MCP. Presumably, the living macrospecies are so long that some terminals of Ru were imbedded in the polymer coils of **PFNP** and hinder them to initiate MCP reaction further, resulting in the formation of diblock copolymer **PFNP**$_{100}$-*b*-**PFHD**$_{50}$

ineffectively.

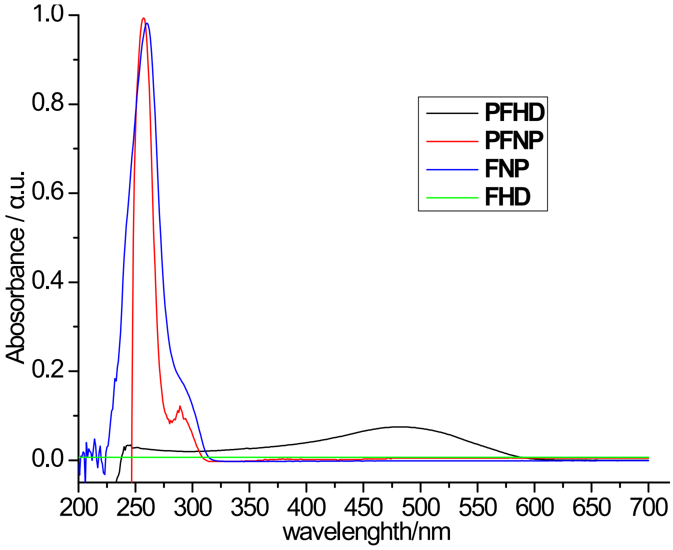

Figure S4. UV-vis absorption spectra of **FHD**, **FNP, PFHD**, and **PFNP** in $CHCl_3$.

In order to ensure MCP of **FHD** occurred with full conversion, we shorten the repeat unit of the first macroinitiator **PFNP** to prepare a series of soluble copolymers in orange to red color corresponding to the increased **PFHD** fraction (Table S1). For all of copolymers, GPC curves showed two distinguished sets of traces (Figure 1b). The major peak is in good accompany with theory M_n of diblock copolymers (M_n^c in Table 1), whereas minor traces with much higher M_n (M_n^d in Table S1) may be corresponded to the aggregates of copolymers as THF is a selective solvent for copolymers.

Structure characterization of polymers and copolymers

In the IR spectrum (Figure S3) of monomers **FNDI** and **FNP**, the absorption bands at 2800-3100 cm^{-1} assigned to the stretching vibration of saturated C-H and unsaturated C=C in NBE and benzene ring pendants. After ROMP, the only change was the transformation of the double bond on NBEs to polyene backbone and no additional absorption was observed in corresponding homopolymers. As for **FHD**, the characteristic absorptions of alkyne at 2120 and 3320 cm^{-1} were corresponded to the stretching vibration of C≡C and unsaturated C≡C–H, respectively. After MCP, heptadiyne monomer transformed to cyclic conjugated backbone. Correspondingly, the absorption of alkyne was completely disappeared and the new absorptions at 2981 and 2850 cm^{-1} were attributed to the methylene in the five-numbered ring and the unsaturated conjugated backbone, respectively. For copolymer **PFNP**$_n$-*b*-**PFHD**$_m$, the curve (Figure S3g) contained both the C-N stretching vibration absorption at 1190 cm^{-1} in **PFNP** and carbonyl stretching vibration absorption at 1780 cm^{-1} in **PFHD**, demonstrating the successful preparation of copolymer via a tandem ROMP-MCP process.

The ^{1}H NMR spectra of **PFNDI** and **PFNP** (Figures S5a and S5b) showed that the signal of olefinic protons on the norbornene ring at about 6.19 ppm is completely disappeared after ring opening, whereas the new signal of olefinic protons on the backbone comes at 5.90-5.40 ppm, which points out polymerization is processed successfully. As shown in previous assignments,[4] the *trans*/*cis* ratio of as-synthesized polymers can be analyzed by integration of the ^{1}H NMR signals related to the vinyl group at 5.90-5.40 ppm and the *trans*/*cis* ratio of **PFNDI** formed by **Ru-III** was 10:9. As comparison, **PFNP** showed a solely absorption of *trans* double bond but no appearance of *cis* double bond. The result demonstrated that comparing with dicarboximide structure, the more rigid pyrrolidine pendant is helpful to tailor high-*trans* configuration in backbone, which may be benefit to improve the dielectric constant.

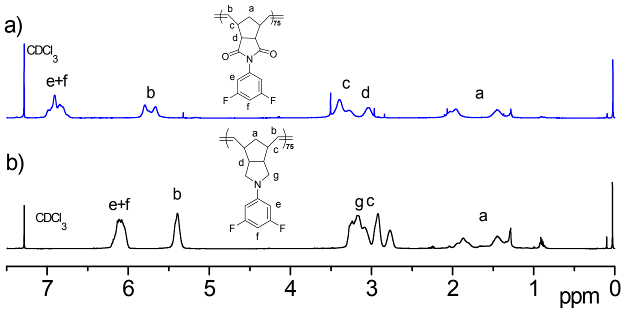

Figure S5. ^{1}H NMR spectra of (a) **PFNDI** and (b) **PFNP**.

Oddly, ^{1}H NMR analysis of soluble block copolymers at room temperature revealed no signals corresponding to the segment of **PFHD** but only signals corresponding to **PFNP** (Figure S6a), even though either UV-vis or FT-IR spectra give a clear indication that **PFHD** bock has successfully attached to the copolymer. Combining the results of GPC analysis, the reason seems to be that the existence of insoluble **PFHD** block would promote the *in situ* self-assembly during the tandem polymerizations, forming micelles consisting of the insoluble **PFHD** block as core and the soluble **PFNP** block as shell. The micelles were stable enough to maintain the self-assembly under the shear pressure of the GPC conditions. Rigid core consisting of **PFHD** segments was not solvated by $CDCl_3$, thus the signals for **PFHD** in ^{1}H NMR spectrum were not detected. By raising the temperature from 25 to 50 °C, the characteristic signals corresponding to the conjugated backbone (H_h) in **PFHD** block was slightly detected (Figure S6b). As the length of **PFHD** increased from 25 to 50, the ^{1}H NMR spectrum of corresponding block copolymer at 50 °C showed more obviously signals (Figure S6c). However, the real block ratio of copolymers could not be calculated by the end-group analysis of ^{1}H NMR spectroscopy because only a small part of **PFHD** signals was solvated and detected (ascribed to the formation of core-shell nanostructure with **PFHD** core tightly enwrapped by **PFNP** shell).

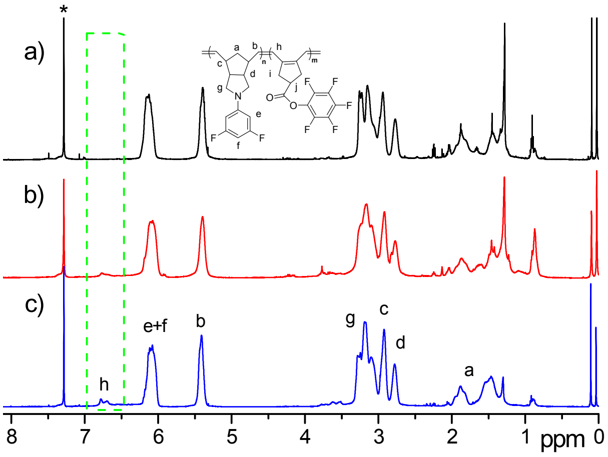

Figure S6. ^{1}H NMR spectra of (a) **PFNP$_{75}$-*b*-PFHD$_{25}$** at 25 °C, (b) **PFNP$_{75}$-*b*-PFHD$_{25}$** at 50 °C, and (c) **PFNP$_{75}$-*b*-PFHD$_{50}$** at 50 °C.

Another effective quantitative analysis for copolymers is the elemental analysis. Since only **PFNP** block contained nitrogen atom, we can obtain the real ratio of **PFNP** block though various nitrogen contents in **PFNP$_n$-*b*-PFHD$_m$** in comparison with homopolymer **PFNP**. On the basis of high activity of **FNP** in ROMP, we calculated the real block ratio in copolymers on condition that **FNP** had completely converted into **PFNP** and the results are listed in Table S2. On the average copolymer chain, the tested block ratio matched well with the monomer feed ratio.

Table S2. The elemental analysis result of copolymers with different block lengths.

Copolymer	N (wt%)	N (wt%)/FW	**PFNP%**	**PFNP**:**PFHD**[a]	**PFNP**:**PFHD**[b]
PFNP$_{50}$-*b*-PFHD$_{25}$	3.49	0.249	61.5	50:25	50:25
PFNP$_{75}$-*b*-PFHD$_{15}$	4.46	0.318	78.63	75:15	75:16
PFNP$_{75}$-*b*-PFHD$_{25}$	4.29	0.306	75.66	75:25	75:20
PFNP$_{75}$-*b*-PFHD$_{50}$	3.22	0.229	56.62	75:50	75:47

[a] The feed block ratio.

[b] The tested block ratio.

Optical properties of copolymers

Except for NMR technique, careful UV−vis analysis may provide additional information on the polymer conformation. The block copolymers showed distinct absorptions as a narrow peak at 240-300 nm for **PFNP** segment and the broad peak at 400-600 nm for **PFHD** segment in $CHCl_3$ (Figure S7a). Two well-resolved absorption maxima at 533-547 nm (0-1) and 575-599 nm (0-0) were observed, indicating that the microstructure of **PFHD** was regular polyenes with exclusively more coplanar, extended, and stiffer five-membered ring structure.[5] The maximum absorption wavelength (λ_{max}) (0-1 transition) of copolymers shifted from 533 to 547 nm in Figure S7a when the **PFHD** block length elongated, indicating the increase of effective conjugation length. Besides, an additional shoulder absorption near 590 nm (0-0 transition), tends to be enhanced as the length of **PFHD** elongated. Comparing the absorption of polymer solution, the UV-vis spectra of copolymer in film state exhibited an obvious red-shift of onset absorption (λ_{abs}) from 625 to 670 nm (Figure S7b), which may be caused by the enhanced π-π stacking of the aromatic pendant in the film formed by spin-coating on quartz plate.

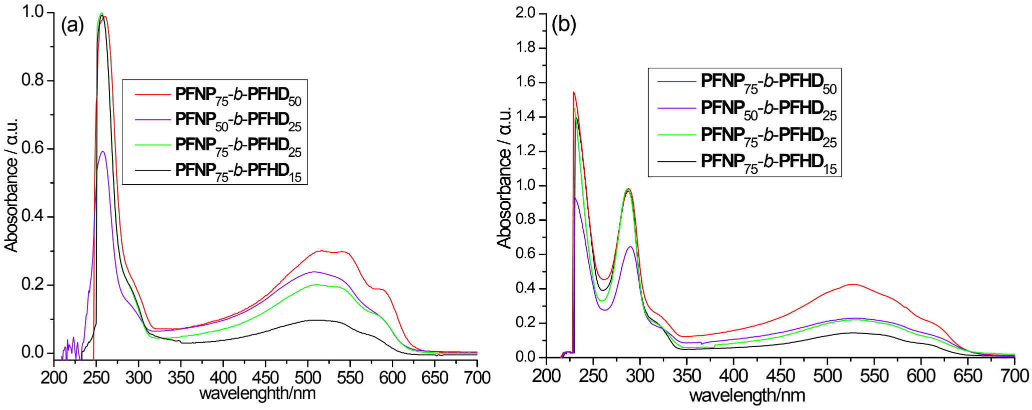

Figure *S7*. UV-vis absorption spectra of copolymers with different **PFHD** lengths (a) in $CHCl_3$ at the concentration of 1.0×10^{-3} mg mL^{-1} and (b) in film state.

Self-assembled nanostructure in solution confirmed by DLS

It was revealed by DLS that a representative copolymer **PFNP**$_{75}$-*b*-**PFHD**$_{50}$ self-assembled into the nanostructures with different average hydrodynamic diameter (D_h) in the selective solvents of THF and $CHCl_3$. In THF (Figure S8a-S8c), the nanostructures have a dominating D_h of 50 nm and another D_h of 200 nm at a diluted concentration of 0.05 mg mL^{-1}; the dominating D_h moved to be 200 nm and another D_h of 70 nm still existed as the concentration increases to 0.5 mg mL^{-1}. For comparison, the nanostructure generated *in-situ* by the polymerization-induced self-assembly in the original THF solution at almost 80 mg mL^{-1} has a single D_h of 200 nm, which is as the same as that formed from the dried copolymer and redissolved in THF. Diversely in $CHCl_3$ (Figure S8d and S8e), **PFNP**$_{75}$-*b*-**PFHD**$_{50}$ formed the nanostructure with a little small D_h of 40 nm at 0.05 mg mL^{-1}; the dominating D_h seems unchanged and a small number of nanostructures with a larger D_h of 200 nm appeared at 0.5 mg mL^{-1}, which may be caused by the aggregation of smaller particles. These results dictated that the self-assembled nanostructures are easily generated, actually stable and reproducible in THF, which presented an evidence to the GPC observation.

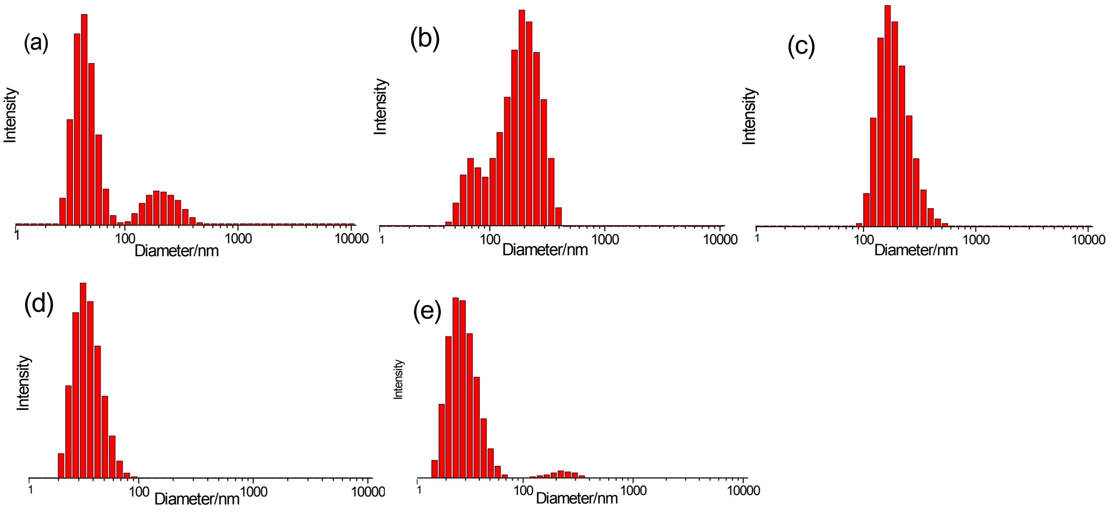

Figure S8. Sizes of copolymer **PFNP$_{75}$-*b*-PFHD$_{50}$** at different concentrations of (a) 0.05, (b) 0.5, and (c) 80 mg/mL (the original reaction solution) in THF; (d) 0.05 and (e) 0.5 mg/mL in CHCl$_3$ determined by means of DLS.

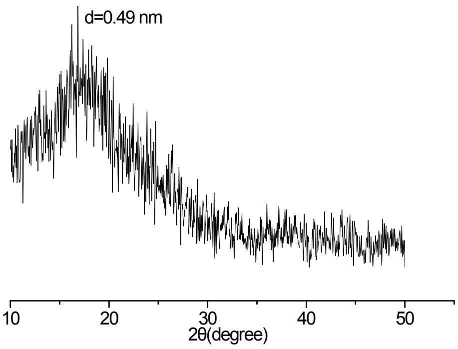

Figure S9. X-ray diffraction pattern of **PFNP$_n$-*b*-PFHD$_m$**.

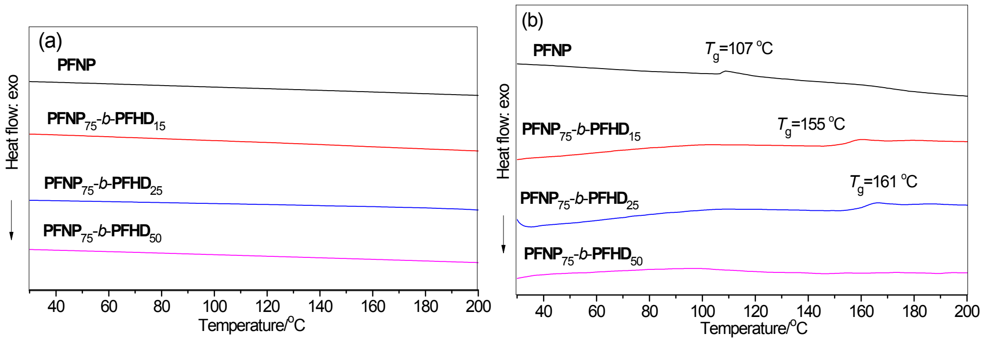

Figure S10. DSC traces of homopolymer and copolymers in (a) the cooling process and (b) the second heating process.

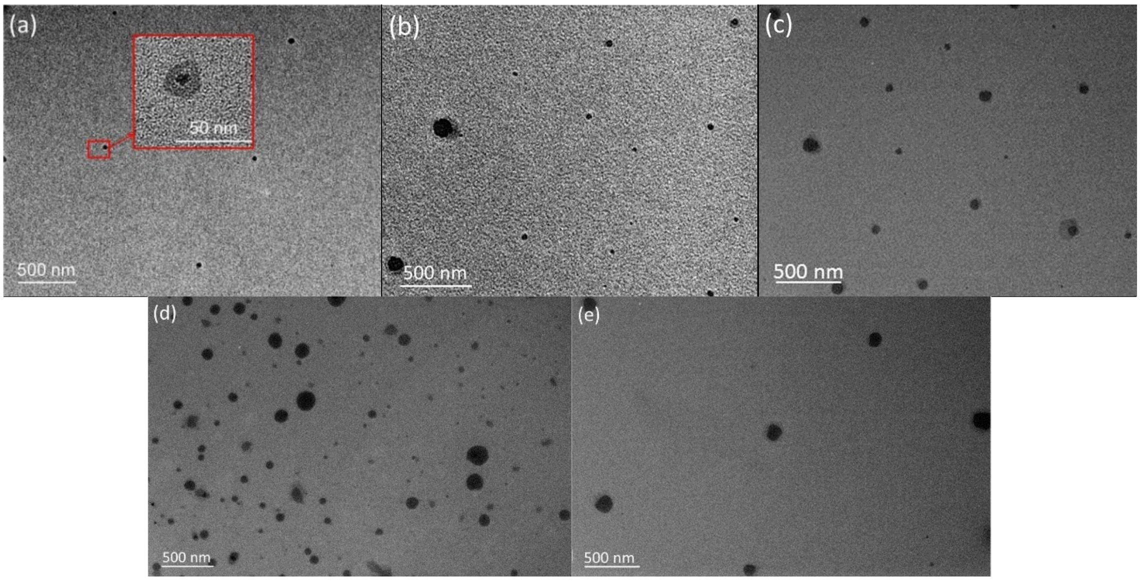

Figure S11. TEM images of **PFNP$_{75}$-*b*-PFHD$_{50}$** at different concentrations of (a) 0.005, (b) 0.05, and (c) 0.2 mg/mL in $CHCl_3$; (d) **PFNP$_{75}$-*b*-PFHD$_{25}$** and (e) **PFNP$_{75}$-*b*-PFHD$_{15}$** at concentration of 0.2 mg/mL in $CHCl_3$.

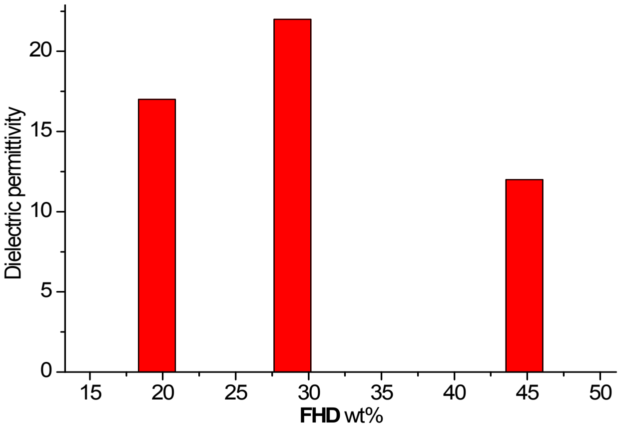

Figure S12. Dielectric permittivity of copolymers **PFNP$_{75}$-*b*-PFHD$_x$** versus **FHD** content (wt%).

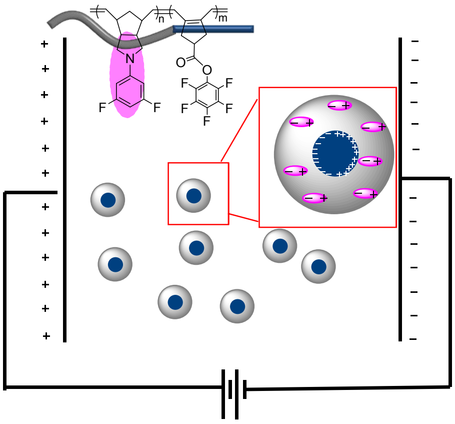

Figure S13. Multiple polarizations in copolymers and their contribution to increasing dielectric permittivity.

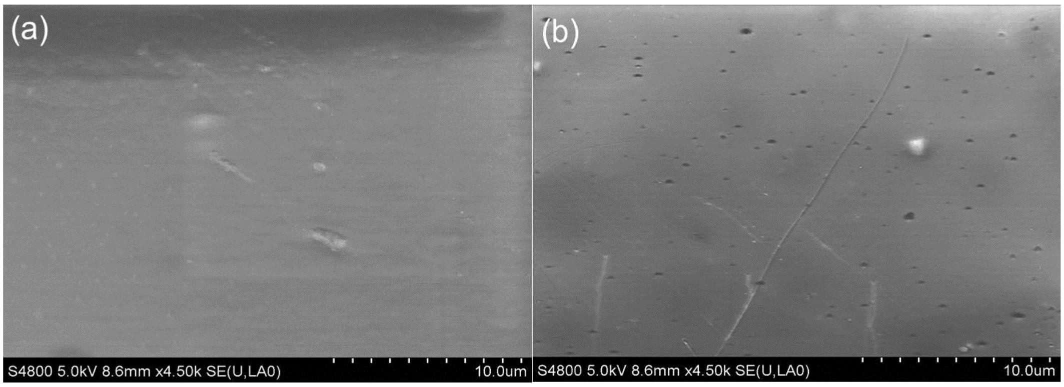

Figure S14. SEM images of polymer film of (a) **PFNP$_{75}$-*b*-PFHD$_{25}$** and (b) **PFNP$_{75}$-*b*-PFHD$_{50}$**.

To apply this unique core-shell structure to improve dielectric performance, the quality of copolymer film was tested by SEM. Since **PFNP** block possesses excellent film-forming property, copolymer film was smooth, homogeneous, and pinhole-free when the rigid **PFHD** block is shorter than 25 units, whereas when the rigid **PFHD** block elongated to 50 units, some air voids and linear aggregates were observed on the surface of film. This poor quality came from the increased content of rigid **PFHD** block and would affect the dielectric property.

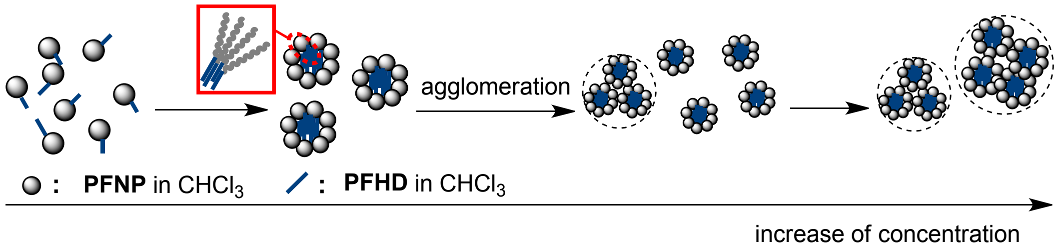

Scheme S1. The schematic process of spherical nanostructure from a single chain of copolymer in $CHCl_3$.

Table S3. Dielectric properties of polymers at 100 Hz-1 MHz.

Polymer	$M_n{}^a$ (kDa)	PDI^a	$K_c{}^b$	tanδ^c
PFNDI	7.8	1.13	5	0.05-0.06
PFNP	20.1	1.11	11	0.04-0.06
PFNP$_{75}$-*b*-PFHD$_{15}$	24.4	1.19	17	0.01-0.02
PFNP$_{75}$-*b*-PFHD$_{25}$	24.8	1.11	22	0.01-0.02
PFNP$_{50}$-*b*-PFHD$_{25}$	23.6	1.18	7	0.01-0.03
PFNP$_{75}$-*b*-PFHD$_{50}$	31.9	1.19	12	0.02-0.04

[a] Determined by GPC in THF relative to monodispersed polystyrene standards.

[b] The dielectric constant of polymer film.

[c] The dielectric loss of polymer film.

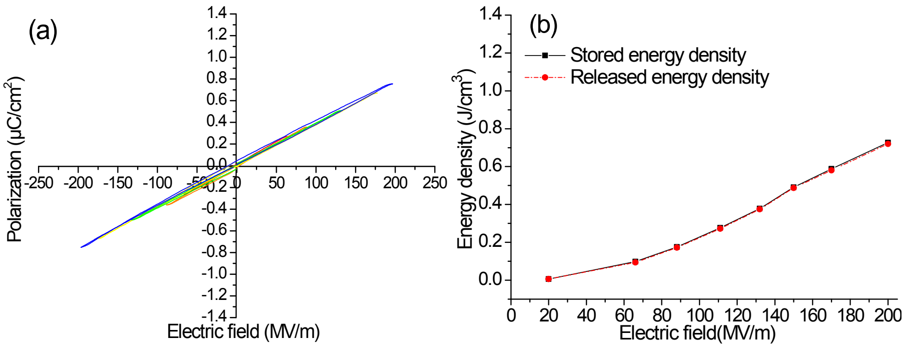

Figure S15. Polarization (D–E) loops (a) and energy density versus applied electric field (b) for **PFNP**.

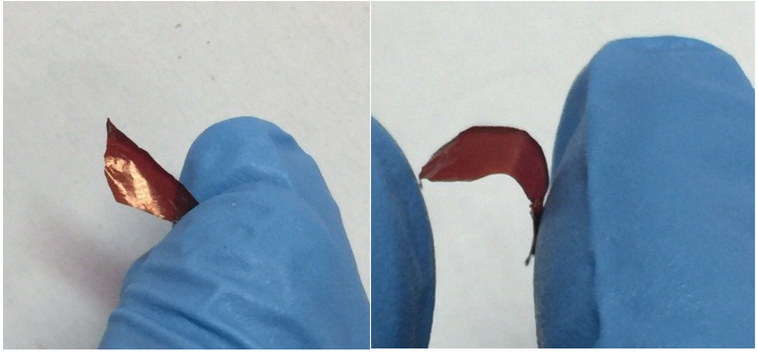

Figure S16. Photographs of free-standing film of **PFNP**$_{75}$-*b*-**PFHD**$_{25}$.

References

1 J. A. Love, J. P. Morgan, T. M. Trnka, R. H. Grubbs, *Angew. Chem., Int. Ed.* **2002**, *41*, 4035-4037.

2 J. M. Carney, P. J. Donoghue, W. M. Wuest, O. Wiest, P. Helquist, *Org. Lett.* **2008**, *10*, 3903-3906.

3 A. A. Santiago, J. Vargas, S. Fomine, R. Gavino, M. A. Tlenkopatchev, *J. Polym. Sci., Part A: Polym. Chem.* **2010**, *48*, 2925-2933.

4 a) Z. You, D. Gao, O. Jin, X. He, M. Xie, *J. Polym. Sci., Part A: Polym. Chem.* **2013**, *51*, 1292-1301; b) G. R. Davies, H. V. St. A. Hubbard and I. M. Ward, *Polymer,* **1995**, *36*, 235. c) G. R. Davies, W. James Feast, V. C. Gibson, H. V. Hubbard, K. J. Ivin, A. M. Kenwright, E. Khosravi, E. L. Marshall, J. P. Mitchell, I. M. Ward, in *Makromolekulare Chemie. Macromolecular Symposia, Vol. 66*, Wiley Online Library, **1993**, pp. 289-296.

5 a) E. H. Kang, I. H. Lee, T. L. Choi, *ACS Macro Lett.* **2012**, *1*, 1098-1102; b) J. O. Krause, M. T. Zarka, U. Anders, R. Weberskirch, O. Nuyken, M. R. Buchmeiser, *Angew. Chem., Int. Ed.* **2003**, *42*, 5965-5969; c) U. Anders, O. Nuyken, M. R. Buchmeiser, K. Wurst, *Macromolecules* **2002**, *35*, 9029-9038.